

# Numerical Study on Influence of Key Parameters of Aerodynamic Characteristics of Shaftless Ducted Rotor

SHEN Suiyuan, ZHU Qinghua\*, WANG Kun, CHEN Jianwei,  
ZENG Jianan, DING Zhengyuan

National Key Laboratory of Rotorcraft Aeromechanics, Nanjing University of Aeronautics and Astronautics,  
Nanjing 210016, P. R. China

(Received 18 June 2019; revised 16 July 2019; accepted 1 September 2020)

**Abstract:** Shaftless ducted rotor (SDR) is a new type of ducted rotor system designed with ducted-rotor-motor integration, which is quite different from traditional ducted rotor (DR) in aerodynamic characteristics. The sliding mesh based on unstructured grid is used to simulate the aerodynamic characteristics of SDR and DR. Then, the effects of five key parameters, namely, the rotor disk height, the number of blades, the spread angle of the duct, the central hole radius and the ducted lip radius on the aerodynamic characteristics of the SDR are investigated. It is found that the same-sized SDR produces a larger total lift than the DR in hovering, but the lift proportion of its duct is reduced. In the forward flight, a large low-speed region is generated behind the SDR duct, and the reflux vortex in blade root above the advancing blade has the trend for inward diffusion. The rotor disk height has similar effects on SDR and DR. Increasing the number of blades can effectively increase the total lift of SDR, which also increases the lift proportion of duct. Increasing the spread angle of the duct will lead to the rotor lift coefficient decrease, reducing the central hole radius can increase the total lift, but the component lift coefficient decreases. Appropriately increasing the ducted lip radius can increase the total lift, which begins to decrease after reaching a certain value.

**Key words:** shaftless ducted rotor; ducted-rotor-motor integration; ducted rotor; sliding mesh; key parameters; aerodynamic characteristics

**CLC number:** V211.3

**Document code:** A

**Article ID:** 1005-1120(2020)05-0682-12

## 0 Introduction

The ducted rotor (DR) is a power device surrounding the rotor with duct. Germany has been studying the DR during the Second World War. So far, there have been lots of researches and applications for DR<sup>[1-9]</sup>. Compared with isolated rotor, the duct can effectively suppress the formation of the rotor blade tip vortex, which improves the effective diameter of the rotor and the air flow through the duct, meanwhile the flow around the leading edge of the duct lip can generate additional lift, resulting in better aerodynamic performance<sup>[10]</sup>.

The tip clearance has a great influence on the aerodynamic performance of the DR. Larger tip

clearance reduces the aerodynamic performance of the DR<sup>[11-14]</sup> while smaller tip clearance presents challenges to the duct processing and the safety during system operation. The central body structure of the DR occupies the inner space of the duct, which limits the effective rotor diameter and causes interference to the DR flow field.

Aiming at the problems with DR, a shaftless ducted rotor (SDR) is proposed with structure based on the shaftless rim thruster<sup>[15-18]</sup> in the ship field. The SDR removes the rotor support shaft system and the center body with the motor installed inside the duct. There is no gap between the rotor and the duct, which rotates together with the rotor of

\*Corresponding author, E-mail address: zhuqinghua@nuaa.edu.cn.

**How to cite this article:** SHEN Suiyuan, ZHU Qinghua, WANG Kun, et al. Numerical study on influence of key parameters of aerodynamic characteristics of shaftless ducted rotor[J]. Transactions of Nanjing University of Aeronautics and Astronautics, 2020, 37(5): 682-693.

<http://dx.doi.org/10.16356/j.1005-1120.2020.05.003>

the motor to replace the axial connection of the DR with a radial connection. The SDR adopts the duct-motor-rotor integrated design to make the lift structure more compact, thereby increasing the duct flow area and reducing the flow resistance. The radial connection of the SDR results in opposite chord length distribution of the blade compared with the DR. The blade section chord near the duct wall of the SDR is longer, resulting in higher rotational speed, so the SDR generates more lift compared to the DR.

In this paper, the aerodynamic characteristics of SDR and DR are numerically simulated using the unstructured grid-based sliding mesh. Firstly, the difference of aerodynamic characteristics between SDR and DR is compared. Then, the influences of five key parameters on the aerodynamic characteristics of SDR are analyzed. This paper can provide reference for the aerodynamic optimization and structural design of SDR.

### 1 Structural Composition of SDR

Fig.1 is a structural diagram of the SDR, which is mainly composed of motor rotor, multi-pole stator, fixed bearing, rotating ring, duct, and rotor. SDR's fixed bearings are mounted on either side of the rotating ring to ensure the axial position of the rotating ring and to transmit the thrust gener-

ated by the rotor. The motor is located between two fixed bearings. The rotating ring connects the rotor to the motor rotor, so that the rotor and the motor are integrated, and the radial connection is used instead of the axial connection of the DR. During the operation, the motor rotor drives the rotor to rotate relative to the multi-pole stator.

## 2 Numerical Computation Method

### 2.1 Governing equation

The three-dimensional compressible flow N-S equation is solved numerically based on the finite volume method. The steady state control equation is

$$\frac{\partial(\rho\theta)}{\partial t} + \text{div}(\rho\mathbf{S}\theta) = \text{div}(\Gamma\text{grad}\theta) + Q \quad (1)$$

where

$$\mathbf{S} = um + vn + wl \quad (2)$$

$$\text{div}\mathbf{S} = \nabla\mathbf{S} = \frac{\partial u}{\partial z} + \frac{\partial(rv)}{r\partial r} + \frac{\partial w}{r\partial\varphi} \quad (3)$$

Therefore, Eq.(1) can be expanded to

$$\begin{aligned} &\frac{\partial(\rho\theta)}{\partial t} + \frac{\partial}{\partial z}(\rho u\theta) + \frac{\partial}{r\partial\varphi}(\rho w\theta) + \\ &\frac{\partial}{r\partial r}(r\rho v\theta) = \frac{\partial}{\partial z}\left(\Gamma\frac{\partial\theta}{\partial z}\right) + \\ &\frac{\partial}{r\partial r}\left(\Gamma\frac{\partial\theta}{r\partial\varphi}\right) + \frac{\partial}{r\partial r}\left(\Gamma r\frac{\partial\theta}{\partial r}\right) + Q \end{aligned} \quad (4)$$

where  $\mathbf{S}$  is the velocity vector, and  $\theta$  the eneral variable.  $u, v, w$  are the axial velocity, the radial velocity and the circumferential velocity in the three-dimensional cylindrical coordinates.  $\Gamma$  is the generalized diffusion coefficient, and  $Q$  the gas phase source term.  $\rho$  is determined by the complete gas state equation. The  $k-\epsilon$  RNG turbulence model is used in this paper.

### 2.2 Model and mesh generation

The specific parameters of the SDR benchmark model in this paper are shown in Table 1. The model is divided into two parts: Static domain and rotating domain. The duct and outer field lie in the static domain, and the rotor and rotating ring is the rotating domain. The flux transfer between the two interfaces is performed by sliding mesh technology. As

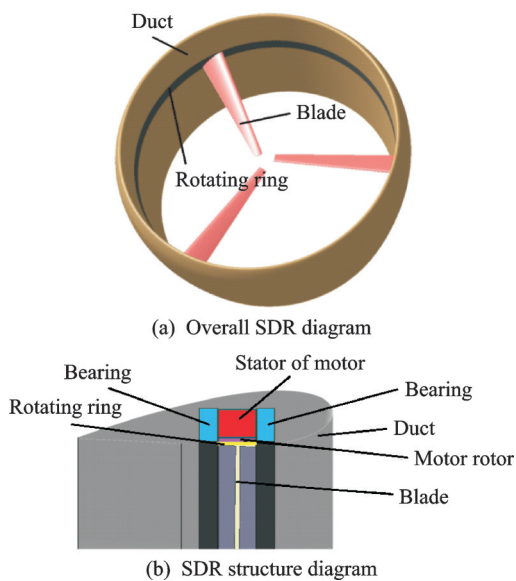


Fig.1 Schema of SDR

shown in Fig.2, the unstructured mesh of the duct and the rotor, in which the duct is simplified, the structure of the stator and the rotor of the rotor in the DR channel is neglected with the rotor and the rotating ring integrated.

**Table 1 Parameters of shaftless ducted rotor**

Parameter	Magnitude
Rotor radius/mm	155
Solidity	0.079
Rotor airfoil	NACA2412
Duct airfoil	NACA0018
Number of blade	3
Blade negative twist/(°)	-27
Spread angle of the duct/(°)	10
Duct radius/mm	168
Height of rotor disk/mm	100
Central hole radius/mm	30
Duct height/mm	150

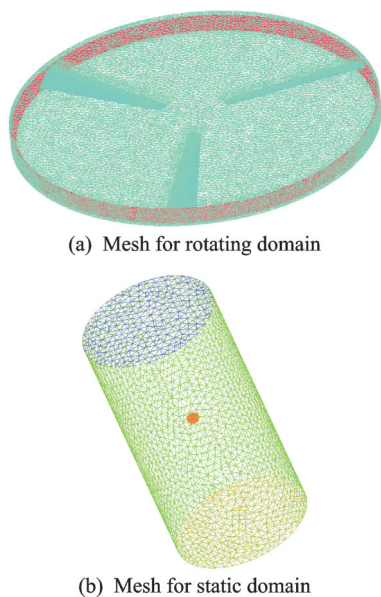


Fig.2 Mesh of shaftless ducted rotor

### 3 Verification of Calculation Method

The TsAGI ducted tail rotor in Ref.[19] is verified by examples. Its specific parameters are shown in Ref. [19]. Figs. 3, 4 show the comparisons between the calculated axial and circumferential velocity calculations and the experimental values<sup>[19]</sup> at the rotor disk. It can be seen that the calculated values of the induced velocity in the two directions are not much different from the experimental values while

sharing similar trends. The numerical calculation result of the rotor disk lift is 85.8 N, which is close to the test value of 90 N in Ref. [19]. The analysis above shows that the numerical calculation method in this paper is reliable and suitable for the later numerical calculation.

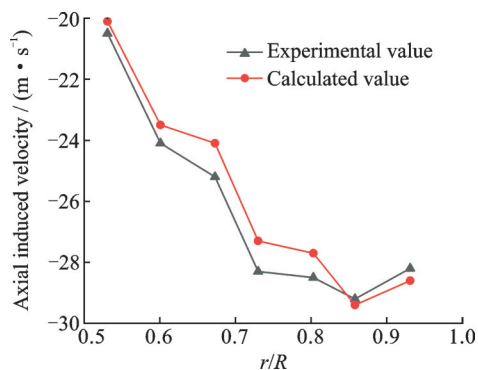


Fig.3 Comparison between calculated and experimental values of axial induced velocity at rotor disk

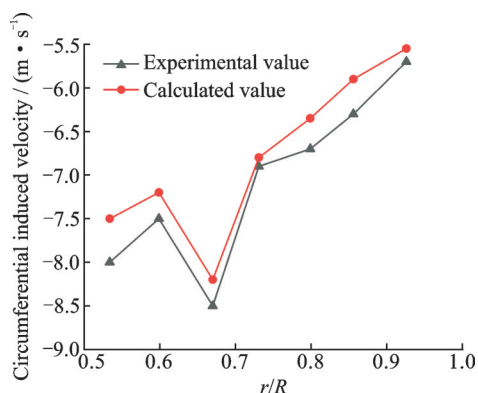


Fig.4 Comparison between calculated and experimental values of circumferential induced velocity at rotor disk

## 4 Results and Analysis

### 4.1 Differences in aerodynamic characteristics between SDR and DR

The benchmark model data in Table 1 is used for the calculation of SDR and DR. The duct airfoil is NACA4415 and the DR hub radius is 30 mm. Fig.5 shows the lift coefficient of each component in two configurations as a function of rotor speed. It can be seen that with the increase of rotor speed, the lift coefficient of each component in the two configurations generally increases and the total lift coefficient of SDR is higher than that of DR. At a rotor speed of 2 000 r/min, the total lift coefficient of

SDR is 1.18 times of DR, which increases to 1.28 at a rotor speed of 12 000 r/min. The lift coefficient of SDR duct is smaller than that of DR. At the same time, it can be seen from Fig.6 that the ratio of duct lift to the total lift for DR is much higher than that of the SDR. When the rotor speed is 2 000 r/min, the ratio of duct lift to the total lift for DR is 1.87 times that of the SDR, which is decreased to 1.66 times as the rotor speed increases to 12 000 r/min, indicating that the ratio of the two configurations decreases with the increase of the rotor speed.

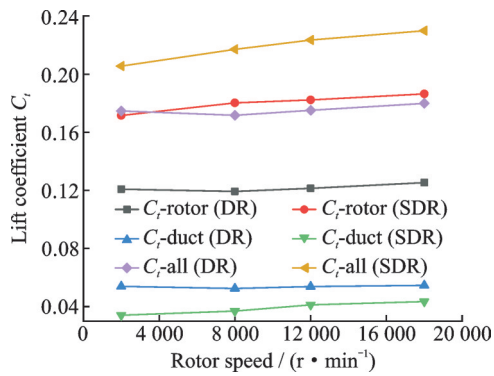


Fig.5 Lift coefficient vs rotor speed

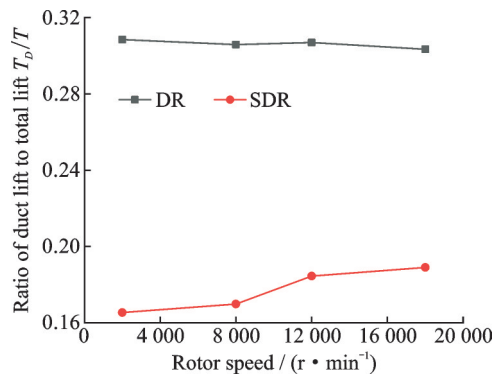


Fig.6 Ratio of duct lift to total lift vs rotor speed

Fig.7 shows the velocity flow diagram of two configurations. It can be seen that due to the presence of the tip clearance, the tip vortex appears at the blade tip which causes flow blockage<sup>[11]</sup>. At the same time, due to the hub blockage, turbulence occurs under the hub. The blade tip vortex and the central turbulence resulting from the hub blockage show a significant improvement on the rotor flow field. However, the tip vortex caused by the tip clearance and the central turbulence formed by the

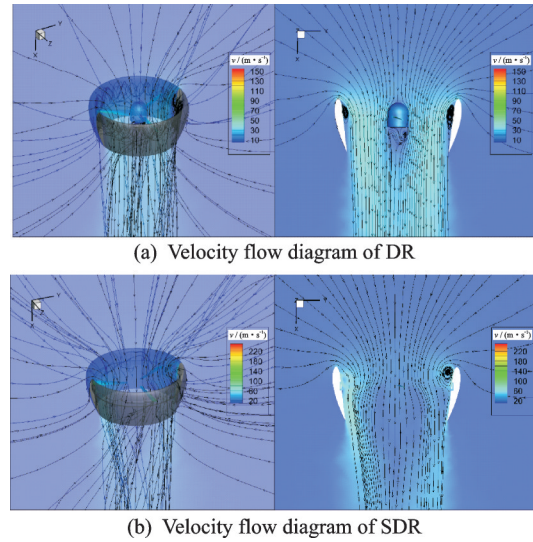


Fig.7 Velocity flow diagram of two configurations

hub will not occur for the SDR, the structure of SDR has a significant improvement on the rotor flow field. The DR draws the external airflow into the duct and then evenly flows out from the outlet, while the SDR draws the external airflow into the duct and then causes airflow shrinkage at the exit. While a reflux vortex in blade root appears near the duct wall on the right side of the rotor, which is because the right side of the section is at the front of the blade, and when it flows upward through the front of the blade, the radial velocity of the blade root is greater. When the chord length is larger, the radial force of the blade will blow the upper stream away, causing it failing to flow smoothly through the rotor disk to form a low pressure vortex.

Fig.8 shows the pressure distribution contour on the upper and lower surfaces of the rotor for the two configurations. It can be seen that the low-pressure zone on the upper surface and the high-pressure zone on the lower surface for the DR rotor are concentrated in the blade tip, where the chord length of the blade section is smaller. While the low-pressure zone on the upper surface and the high-pressure zone on the lower surface for the SDR rotor are concentrated in the blade root, where the chord length of the rotor section is larger, and the pressure difference between the upper and lower surfaces is larger than that of DR, resulting in larger rotor lift coefficient.

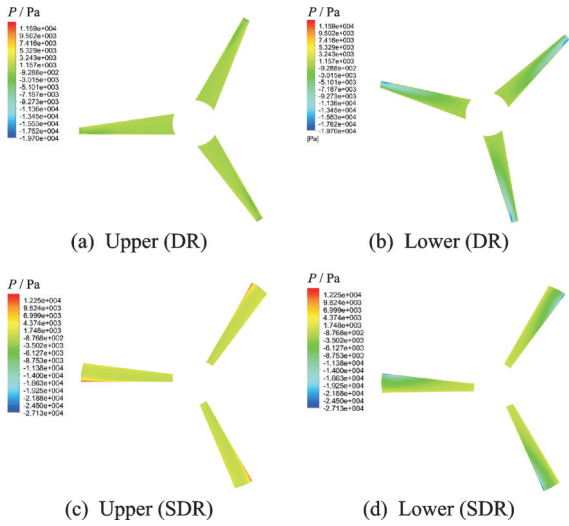


Fig.8 Pressure distribution contour on upper and lower surfaces of rotor

Fig.9 shows the vertical velocity of the central axis of the two configurations, and the horizontal axis indicates the rotor disk height. It can be seen that there is a negative velocity reverse flow zone from  $0.5R$  to the rotor disk, and there is no reverse flow zone in the SDR. After the  $0.5R$  below the rotor disk, the DR central axis flow rate rises rapidly, while the SDR central axis flow rate is falling, which starts to rise after more than  $1.7R$ .

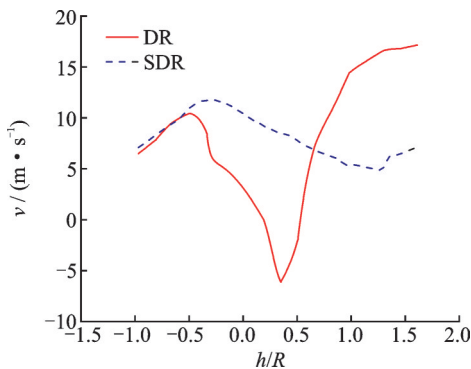


Fig.9 Vertical velocity of central axis

Given a vertical flow  $v=10$  m/s, a velocity streamline diagram as shown in Fig.10 is obtained. It can be seen that the DR and SDR streamlines tend to be perpendicular. The tip vortex in the DR disappears, and the wake vortex appears on the duct wall below the rotor disk, and the reflux vortex in blade root above the right-hand rotor of the SDR disappears, which is because the vertical velocity of the incoming flow increases and the effect of the

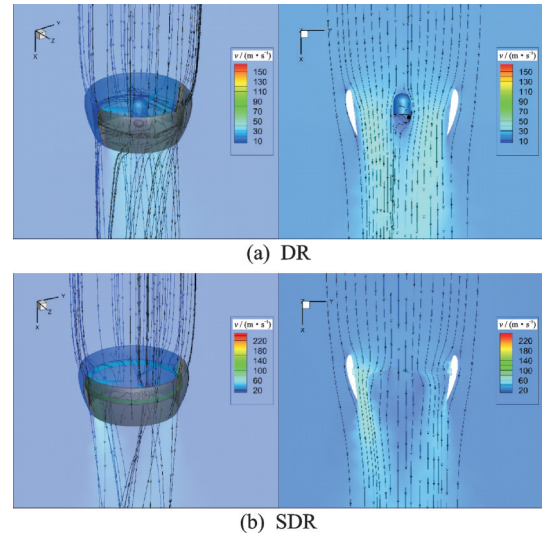


Fig.10 Velocity streamline diagram under vertical flow

blade radial force reduces.

Given an inclined flow  $v=17$  m/s, direction angle  $\alpha=30^\circ$ , a velocity streamline diagram as shown in Fig.11 is obtained. It can be seen that the tip vortex on the right side of the DR duct disappears, and the low-pressure vortex is formed on the left side of the duct. At the same time, due to the blockage of the duct, a low-speed zone is formed behind the duct, the SDR also has a low-speed zone with larger area, and the reflux vortex in blade root on the right side of the rotor has an inward diffusion tendency.

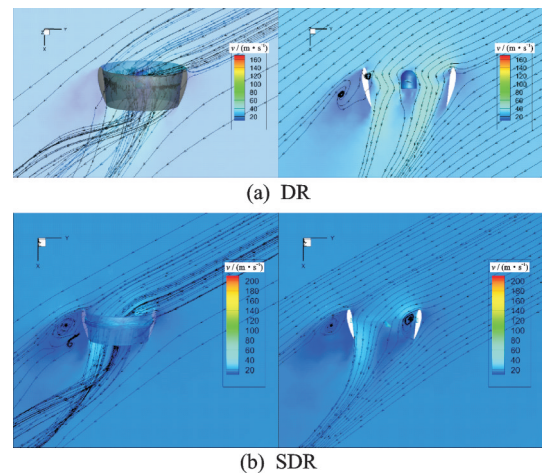


Fig.11 Velocity streamline diagram under inclined flow

#### 4.2 Influence of rotor disk height

For DR, the rotor disk height ( $h$ ) has the most optimal lift performance at approximately  $1/3$  of the duct height ( $H$ )<sup>[20]</sup>. For the SDR, the overall aero-

dynamic performance in the case of different rotor disk heights in hovering is compared using the benchmark model of Table 1. The rotor speed is 12 000 r/min.

Fig. 12 shows the SDR lift coefficient and the rotor torque coefficient as a function of the rotor disk height. The abscissa represents the height difference between the rotor disk and the duct inlet. It can be seen that the lift coefficient of the rotor and the duct share similar change trends, and  $1/4H$  to  $1/3H$  is the rising section while  $1/3H$  to  $1/2H$  is the descending section. When the rotor disk height exceeds  $1/2H$ , the lift coefficient starts to rise. When the rotor disk height is  $1/3H$ , the total lift coefficient is 1.25 times of that in  $1/2H$  while the torque coefficient is 0.98 times of that in  $1/2H$ . The rotor torque coefficient does not change much before the rotor disk height goes up to  $2/3H$ , but plunge to 0.85 times of that in  $1/4H$  when rising to  $3/4H$ .

Fig. 13 shows the trend of the ratio of the duct lift to the total lift as a function of rotor disk height. It can be seen that the ratio of duct lift to total lift and the lift coefficient have the similar changes as the rotor disk height varies, which rises to 36.4% at  $1/3H$  and descends to 27.5% at  $1/4H$ .

The above calculation results show that the ro-

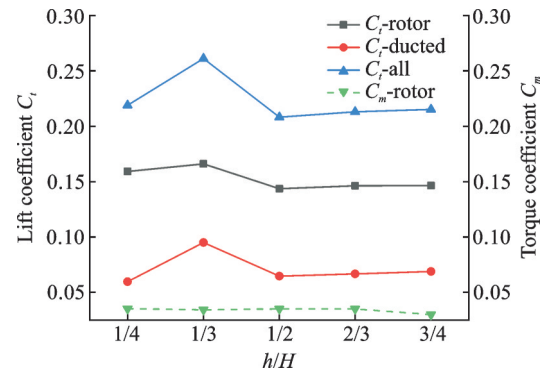


Fig.12 Rotor lift coefficient and torque coefficient with respect to rotor disk height

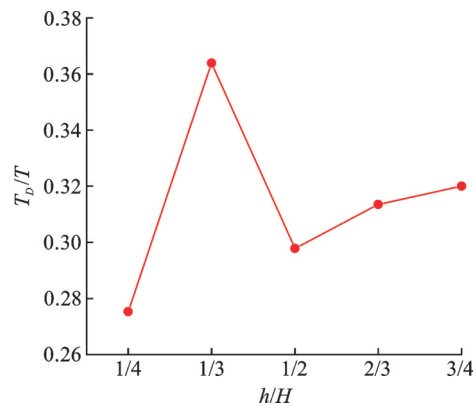


Fig.13 Ratio of duct lift to total lift with respect to rotor disk height

tor disk height has similar effect on SDR and DR, and the optimal height is around  $1/3H$ .

It can be seen from Fig.14 that the reflux vor-

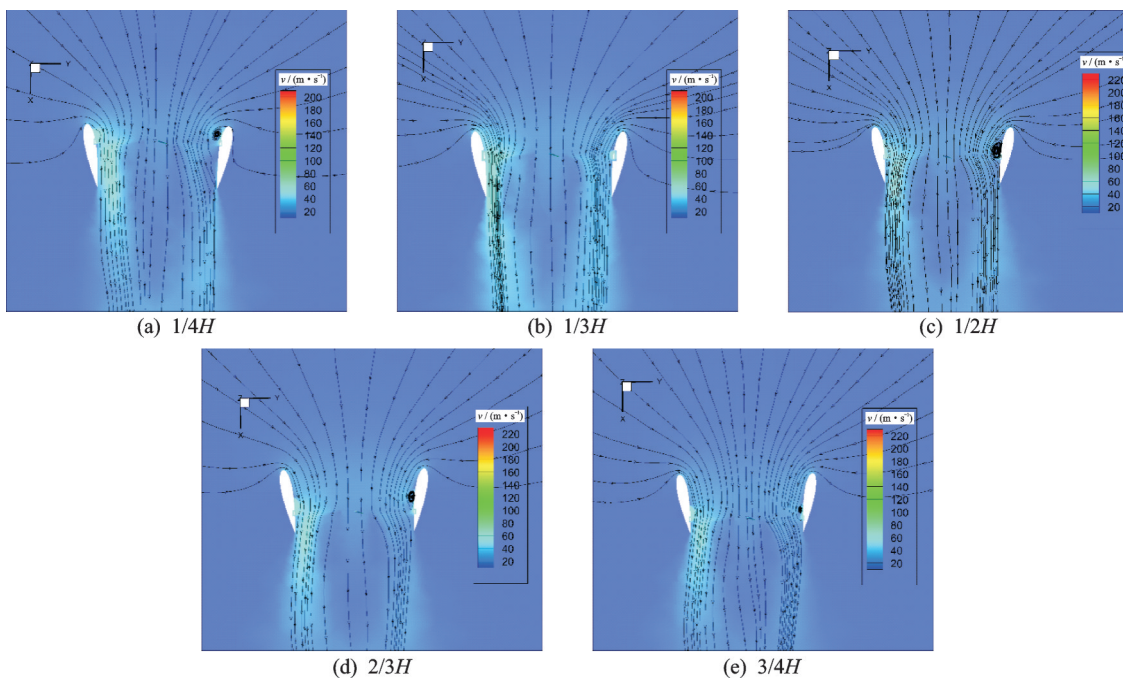


Fig.14 Section velocity flow diagram in duct varying rotor disk height

tex in blade root on the right side of the rotor moves with the movement of the rotor disk, which disappears at  $1/3H$ . There is a strong reflux vortex in blade root at  $1/2H$ . When the rotor disk height increases, its strength gradually weakens. The reflux vortex in blade root nearly disappears when the height increases to  $3/4H$ , indicating that the reflux vortex in blade root over the rotor has a great influence on the aerodynamic performance of the rotor, the smaller the reflux vortex in blade root, the larger the lift coefficient of the rotor.

### 4.3 Influence of number of blades

Based on the model in Table 1 with a rotor disk height of  $1/2H$ , calculations in Cases of 2, 3, 4 blades are carried out at a rotor speed of 12 000 r/min.

Fig. 15 shows that with the number of blades increasing, the lift coefficient of each component and the torque coefficient of the rotor increase. The total lift coefficient of four blades is 1.54 times of that for two blades, and the rotor torque coefficient is 1.38 times. Fig. 16 shows the ratio of duct lift to total lift in the case of different number of blades. It can be seen that the higher the number of blades is, the higher the ratio of the duct lift to the total lift is. The ratio of the duct lift to the total lift for 4 blades is 1.43 times as much as that of 2 blades.

Fig. 17 is a section velocity flow field diagram in duct with different blade numbers. It can be seen that the flow field of the two blades is more chaotic. After the airflow passes through the rotor disk plane, it rapidly spreads to both sides and then converges beneath the duct, causing a recirculation

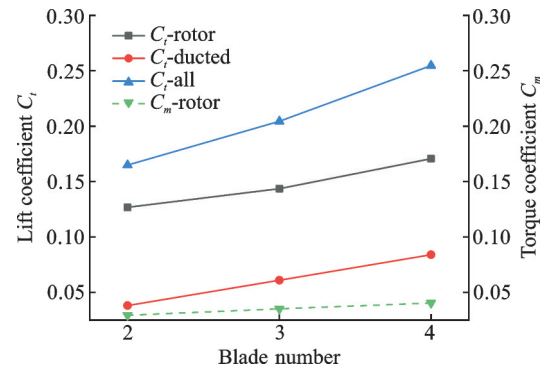


Fig. 15 Rotor lift coefficient and torque coefficient with respect to number of blades

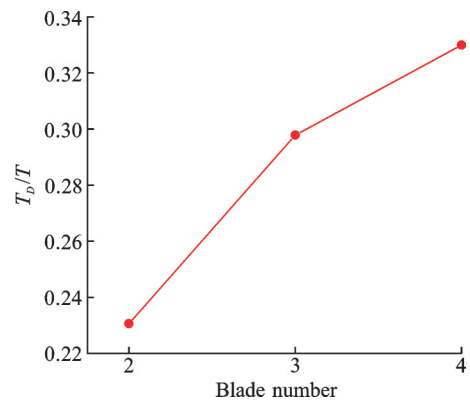


Fig. 16 Ratio of duct lift to total lift with respect to number of blades

zone below the middle of the rotor disk, which leads to the descending of the pressure difference between the upper and lower surfaces of the rotor, and decreasing of rotor lift. When the number of blades is an even number, the reflux vortex in blade root is formed on both sides of the rotor because of the both sides of the section being at the front of the blade. When the number of blades increases, the strength of the reflux vortex in blade root is weakened, which leads to the fluent flow inside the duct, and finally results in the improvements of the aero-

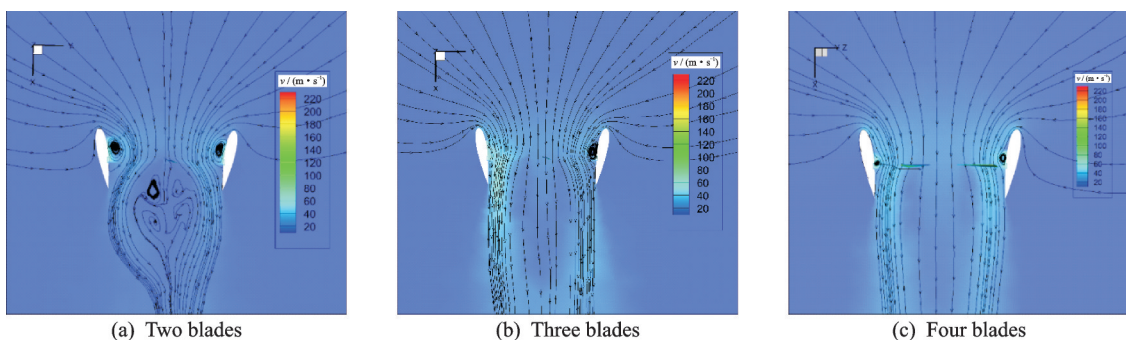


Fig. 17 Section velocity flow field diagram in duct with respect to number of blades

dynamic performance.

Fig. 18 is rotor middle section pressure contour in the case of different blade number. It can be seen from the picture that the pressure distribution of

even blades is symmetrical, while that of odd blades is asymmetrical. The low-pressure area under the rotor disk presents an external triangular diffusion area, which increases the rotor lift.

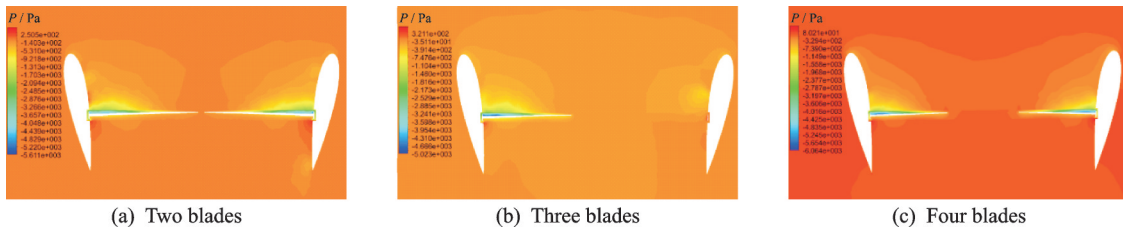


Fig.18 Rotor middle section pressure contour diagram in case of different blade numbers

#### 4.4 Influence of spread angle of ducted

The spread angle of duct is an important parameter in DR design. Appropriate expansion of spread angle of duct can improve the aerodynamic performance of DR<sup>[20]</sup>. To study the influence of spread angle of duct on aerodynamic characteristics of SDR, the model in Table 1 is selected as the reference model and the rotor speed is 12 000 r/min. Calculations for spread angle of duct of 0°, 6° and 10° are carried out.

Fig. 19 shows the relationship between the rotor lift coefficient and torque coefficient as a function of the spread angle of duct. It can be seen that as the spread angle of duct increases, the rotor and total lift coefficient decrease. The total lift coefficient decreases by 12.4% from 0.298 to 0.261 while the rotor torque coefficient decreases by 33.7% from 0.046 6 to 0.030 9. The duct lift coefficient rises first and then decreases. From the relationship between the total lift force ratio and the spread angle

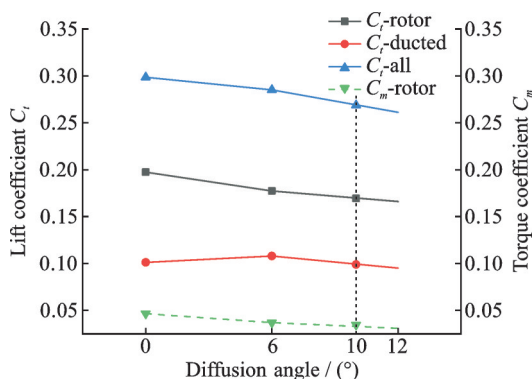


Fig.19 Rotor lift coefficient and moment coefficient with respect to spread angle of duct

of duct in Fig.20, it can be seen that in the case of spread angle of duct 6°, the ratio of duct lift reaches the maximum of 37.8%. The above calculation result shows that the expansion of the spread angle of duct does not improve the aerodynamic performance of SDR, which differs from that for DR.

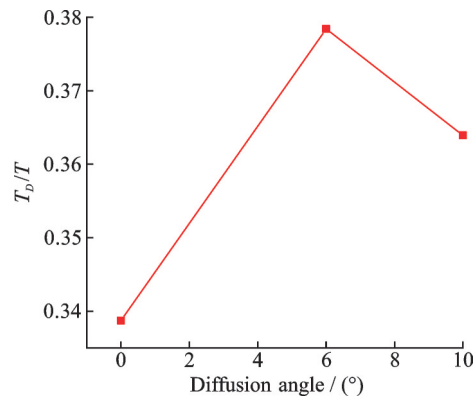


Fig.20 Ratio of duct lift to total lift with respect to spread angle of duct

Fig.21 is a cross-section velocity flow diagram in different spread angle of duct, and Fig.22 is section velocity contour diagram. It can be seen that as the spread angle of duct increases, the low velocity region in axial plane has an inward contraction tendency. Both of the duct inlet and outlet flow velocity rise, which indicates that increasing of spread angle of duct and narrowing the outlet will lead to the airflow gathering inside. The gathering of flow blocks the rotor wake, and deflects the middle airflow, which causes the reducing of airflow at the blade root and the decreasing of rotor lift.

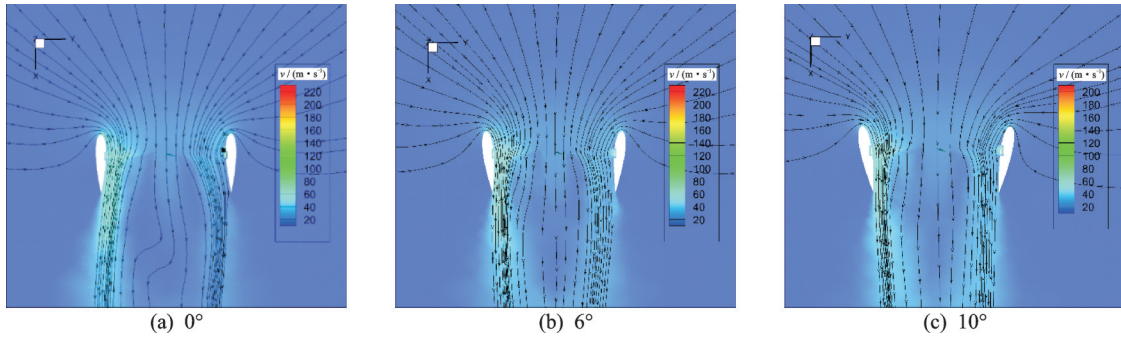


Fig.21 Cross-section velocity flow diagram in different spread angle of duct

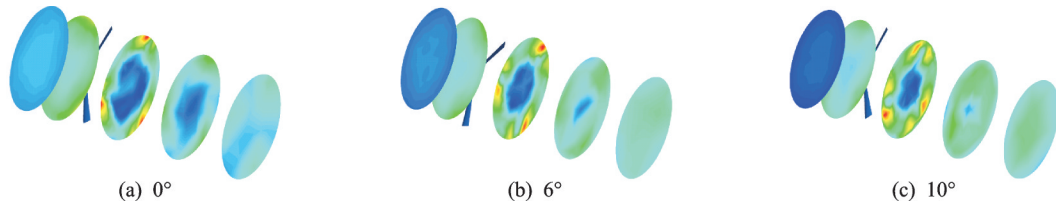


Fig.22 Section velocity contour diagram at different heights

**4.5 Influence of the central hole radius**

The SDR removes the central component of the DR in terms of structural design, so its central hole radius can be reduced to increase the effective diameter of the rotor. The data model in Table 1 is selected as the reference model. NACA66 is used for the duct airfoil, and the central hole radius of 10, 20 and 30 mm is calculated.

Figs.23, 24 show the rotor lift coefficient, and torque coefficient and the total lift as a function of the central hole radius. It can be seen that the rotor torque coefficient does not change much when the central hole radius changes with the amplitude within 3.6%. The reduction of the central hole radius can increase the total lift because of the increasing of the effective diameter of the rotor. The total lift co-

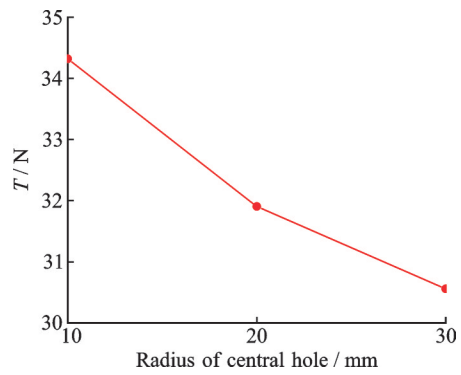


Fig.24 Total lift vs central hole radius

efficient reaches the maximum at 0.193 when the central hole radius is 20 mm. The lift coefficient does not increase as the central hole radius decreases. The ratio of duct lift to total lift with respect to central hole radius is shown in Fig. 25. When the central hole radius is 20 mm, the duct lift ratio is

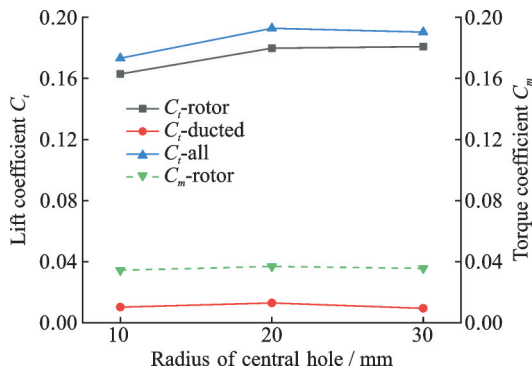


Fig.23 Rotor lift coefficient and torque coefficient vs central hole radius

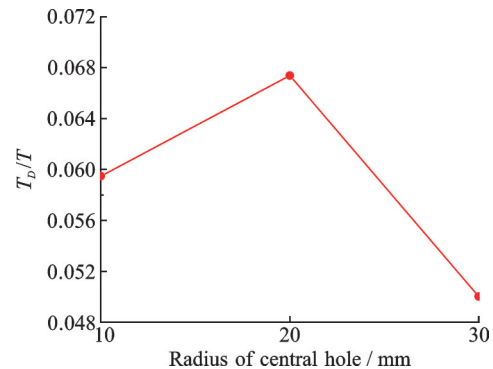


Fig.25 Ratio of duct lift to total lift with respect to central hole radius

0.067 4. Compared with NACA0018, the duct airfoil adopted NACA66 has a large drop in duct lift. Because NACA66 is an arched back airfoil with a small lip radius, it leads to a small additional lift generated by the flow around the lip.

Fig. 26 is a middle-cross-section velocity flow diagram in case of different central hole radius. Fig. 27 shows the vertical velocity of central axis, and the abscissa represents the distance from the rotor disk. It can be seen that increasing the central

hole radius can reduce the reflux vortex in blade root on the right side of the rotor. The flow velocity in the model with three central hole radii is not much different before passing through the rotor disk. However, after passing through the rotor disk the flow velocity of the central hole radius of 10 mm reduces rapidly, which indicates that the larger the central hole radius is, the smoother the flow can pass through the rotor disk, thus weakening the blockage effect of the rotor.

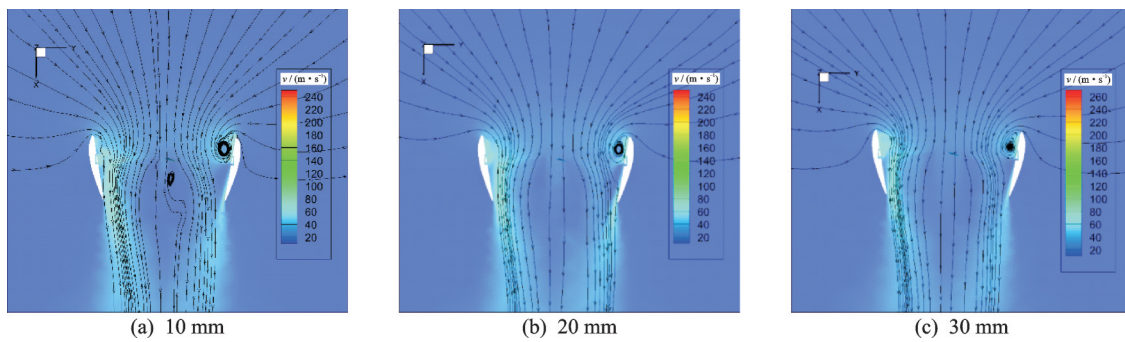


Fig.26 Cross-section velocity flow diagram in case of different central hole radii

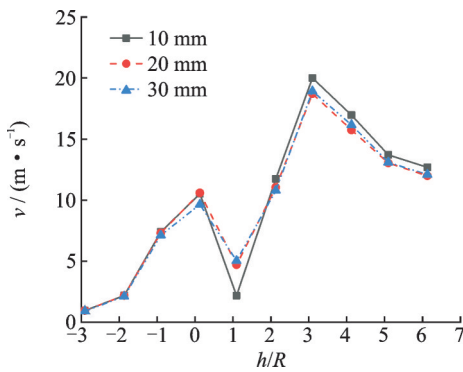


Fig.27 Vertical velocity of central axis

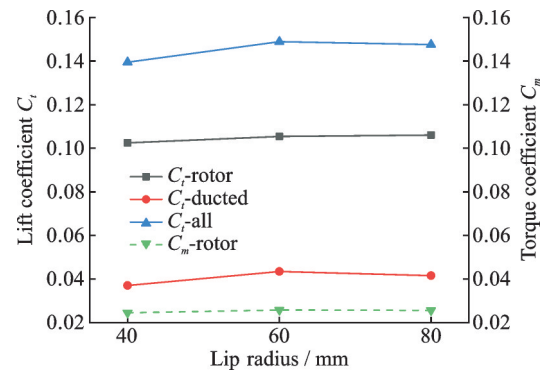


Fig.28 Rotor lift coefficient and torque coefficient with respect to ducted lip radius

#### 4.6 Influence of ducted lip radius

The flow around the leading edge of the ducted lip can generate additional lift. Appropriately increasing the ducted lip radius can increase the duct lift of the DR<sup>[20]</sup>. TsAGI duct and rotor data in Table 1 are used to calculate three ducted lip radii of 40, 60, and 80 mm.

Fig.28 shows the rotor lift coefficient and torque coefficient with respect to ducted lip radius. It can be seen that when the ducted lip radius increases from 40 mm to 60 mm, the total lift coefficient increases by 6.76%. However, when the ducted lip radius continues to increase from 60 mm to

80 mm, the total lift coefficient decreases by 0.87%, which indicates that appropriately increasing the ducted lip radius can increase the rotor and duct lift coefficient, but keep increasing the ducted lip radius will not lead to the increasing of lift coefficient. From Fig.29, it can be seen as the ducted lip radius increases from 20 mm to 40 mm, the ratio of duct lift to total lift rises from 26.54% to 29.19% while the ducted lip radius increases from 40 mm to 60 mm, the ratio descends from 29.19% to 28.1%. This means that if the ducted lip radius increases too much, the duct lift ratio will not continue to rise.

The change in the ducted lip radius has little effect on the rotor torque coefficient, and the changing rate does not exceed 0.5%.

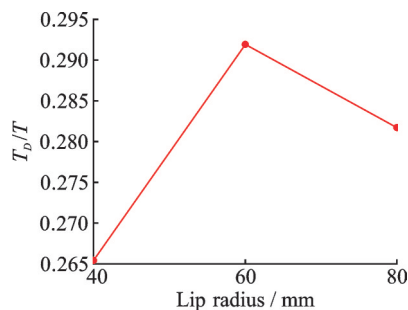


Fig.29 Ratio of duct lift to total lift with respect to ducted lip radius

## 5 Conclusions

In this paper, the aerodynamic characteristics of SDR and DR are numerically simulated using the non-structural grid-based sliding grid. Firstly, the difference of aerodynamic characteristics between SDR and DR is compared. Then, the influences of five key parameters on the aerodynamic characteristics of SDR are analyzed. The following conclusions are obtained:

(1) The same-sized SDR can produce a larger total lift than the DR in hovering, but its duct lift ratio will decrease; in the hovering state, the SDR will not produce the tip vortex but will produce reflux vortex in the blade root near the duct wall, and the reflux vortex causes the duct lift to decrease. When there is a certain axial velocity, the reflux vortex in the blade root disappears. In the forward flight state, there is a bigger low-speed zone behind the SDR duct, the vortex above the leading blade has a tendency to spread inward.

(2) The rotor disk height has a great influence on the aerodynamic performance of the SDR. SDR with a rotor disk height of  $1/3H$ , the maximum total lift occurs, which is similar to the DR.

(3) Increasing the number of blades can effectively increase the total lift of SDR, and the proportion of duct lift tension increases as the number of blades increases. Increasing the duct diffusion angle will cause the SDR rotor lift coefficient to decrease, and the duct lift coefficient is increased first and then decreased.

(4) Reducing the central hole radius can increase the total lift, but the component lift coefficient is decreasing. Increasing the central hole radius can reduce the blockage effect of the rotor on the air flow. Appropriately increasing the radius of the duct lip can increase the total lift, but the total lift begins to decrease when it exceeds a certain value.

SDR is a new type of DR thrust system. Through the above research, it is found that it has certain advantages in aerodynamic performance compared with DR. The next step is to carry out SDR structure and aerodynamic optimization design. In terms of aerodynamics, it is necessary to consider the parameter interaction to find the optimal combination.

## References

- [1] KRIEBEL A R. Predicted and measured performance of two full-scale ducted propellers: NO. CR578[R]. USA: NASA, 1966.
- [2] OSGAR J O III, PAUL A G. A compact method for modeling the aerodynamics of ducted fan vehicles: AIAA-2010-1052[R]. USA: AIAA, 2010.
- [3] TIMOTHY E L. Design and performance of a ducted coaxial rotor in hover and forward flight[D]. Maryland: University of Maryland, 2010.
- [4] XU H Y, YE Z Y. Numerical simulation and comparison of aerodynamic characteristics between ducted and isolated propellers[J]. Journal of Aerospace Power, 2011, 26(12): 2820-2825. (in Chinese)
- [5] PEREIRA J L. Hover and wind-tunnel testing of shrouded rotors for improved micro air vehicle design[D]. Maryland: University of Maryland, 2008.
- [6] PEREIRA J L, CHOPRA I. Hover test of micro aerial vehicle-scale shrouded rotors Part I: Performance characteristics[J]. Journal of American Helicopter Society, 2009, 54(1): 012001-1-012001-28.
- [7] CAI H M, ANG H S, DUAN W B. Design of a new ducted fan aircraft and its aerodynamic characteristic research[J]. Acta Armamentarii, 2012, 33(7): 857-863.
- [8] FAN Y, ZHU Q H. General layout/flight control integrated design for novel ducted quadrotor aircraft[J]. Journal of Nanjing University of Aeronautics & Astronautics, 2017, 49(2): 231-238. (in Chinese)
- [9] XU H Y, YE Z Y. Numerical simulation of ducted-propeller system using unstructured overset grids[J]. Acta Aerodynamica Sinica, 2013, 31(3): 306-309.
- [10] YE K, YE Z Y, QU Z. Aerodynamic optimization method for duct design[J]. Journal of Aerospace Power, 2013, 28(8): 1828-1835. (in Chinese)

- [11] SU Y D, YE Z Y, XU H Y. Influence of tip clearance and propeller separation space on aerodynamic performance of ducted propeller[J]. Journal of Aerospace Power, 2014, 29(6): 1468-1475. (in Chinese)
- [12] MARTIN P, TUNG C. Performance and flow field measurements on a 10-inch ducted rotor VTOL UAV[C]//Proceedings of the 60th Annual Forum of the American Helicopter Society. Baltimore: AHS, 2004: 88-107.
- [13] WU C L, LIU Q Z, HU C B. Principles of turbomachinery[M]. Xi'an: Northwestern Polytechnical University Press, 2009. (in Chinese)
- [14] WU Y H, CHU W L, ZHANG Y F, et al. The influence of tip clearance size on axial compressor rotor aerodynamics: AIAA-2008-85 [R]. USA: AIAA, 2008.
- [15] TAN W Z, YAN X P, LIU Z L, et al. Technology development and prospect of shaftless rimdriven propulsion system[J]. Journal of Wuhan University of Technology (Transportation Science & Engineering), 2015, 39(3): 601-605. (in Chinese)
- [16] WANG Y, LI Q. Design of a new integrated motor propulsion system[J]. Chinese Journal of Ship Research, 2011, 6(1): 82-85. (in Chinese)
- [17] YU Z M, WANG R Z, MENG X Q. Design of underwater detector based on unpowered propulsion and shaftless rim-driven propulsion[J]. Ship Science and Technology, 2017, 39(23): 26-29.
- [18] WU Y. Design and fabrication of a maneuverable robot for in-pipe leak detection[D]. Massachusetts: Massachusetts Institute of Technology, 2014.
- [19] BOURTSEV B N, SELEMENEV S V. Fan-in-fin performance at hover computational method[C]//Proceedings of the 26th European Rotorcraft Forum. The Hague, The Netherlands: [s.n.], 2000.
- [20] LI B. Research on technologies of high-speed ducted-rotor UAV preliminary design[D]. Nanjing: Nanjing University of Aeronautics and Astronautics, 2012. (in Chinese)

**Acknowledgements** This work was supported by the National Defense Science and Technology Key Laboratory Fund (No. 6142220180511) and Priority Academic Program Development of Jiangsu Higher Education Institutions.

**Authors** Mr. SHEN Suiyuan is a Ph.D. candidate who majors in aircraft design in Nanjing University of Aeronautics and Astronautics. His research focuses on the unmanned helicopter flight control and overall and aerodynamic design of rotorcraft.

Dr. ZHU Qinghua received his Ph.D. degree from Nanjing University of Aeronautics and Astronautics in 2008. His research has focused on the overall design of rotor aircraft and helicopter flight dynamics.

**Author contributions** Mr. SHEN Suiyuan designed the study, completed the analysis and wrote the main part of the manuscript. Dr. ZHU Qinghua contributed to background of the study and modified the manuscript. Mr. WANG Kun conducted the analysis and wrote the part of the manuscript. Mr. CHEN Jianwei contributed to data analysis. Mr. ZENG Jianan contributed to discussion and revision of the study. Mr. DING Zhengyuan contributed to result interpretation and manuscript revision. All authors commented on the manuscript draft and approved the submission.

**Competing interests** The authors declare no competing interests.

(Production Editor: SUN Jing)

## 无轴涵道旋翼气动特性数值研究

申遂愿, 朱清华, 王 坤, 陈建炜, 曾嘉楠, 丁正原

(南京航空航天大学直升机旋翼动力学国家级重点实验室, 南京 210016, 中国)

**摘要:** 无轴涵道旋翼 (Shaftless ducted rotor, SDR) 是一种采用涵道-旋翼-电机一体化设计的新型涵道旋翼系统, 其与传统涵道旋翼 (Ducted rotor, DR) 气动特性有较大差异。基于非结构网格的滑移网格技术, 首先分析了 SDR 与 DR 气动特性差异, 然后分别考察了桨盘高度、桨叶片数、涵道扩散角、中心孔径及涵道唇口半径 5 个关键参数对 SDR 气动特性的影响。研究发现: 相同尺寸 SDR 比 DR 在悬停状态能够产生更大的总拉力, 但其涵道拉力占比减小。前飞状态下 SDR 涵道后方产生较大的低速区, 前行桨叶上方涡环有向内扩散趋势。桨盘高度对 SDR 与 DR 的影响机理相似。增加桨叶片数能够有效提高 SDR 的总拉力值, 也能提高涵道拉力占比。增大涵道扩散角将导致 SDR 旋翼拉力系数下降。减小中心孔径能提高总拉力, 但各部分拉力系数在下降。适当增加涵道唇口半径能够提高总拉力大小, 超过一定值后总拉力开始下降。

**关键词:** 无轴涵道旋翼; 涵道-旋翼-电机一体化; 涵道旋翼; 滑移网格; 关键参数; 气动特性